Aspartoacylase is a regulated nuclear-cytoplasmic enzyme

Jeremy R. Hershfield,* Chikkathur N. Madhavarao,* John R. Moffett,* Joyce A. Benjamins,† James Y. Garbern,†,‡ and Aryan Namboodiri*,[1]

*Department of Anatomy, Physiology, and Genetics, The Uniformed Services University of the Health Sciences, Bethesda, Maryland, USA; †Department of Neurology, Wayne State University School of Medicine, Detroit, Michigan, USA; ‡Center for Molecular Medicine and Genetics, Wayne State University School of Medicine, Detroit, Michigan, USA

ABSTRACT **Mutations in the gene for aspartoacylase (ASPA), which catalyzes deacetylation of *N*-acetyl-L-aspartate in the central nervous system (CNS), result in Canavan Disease, a fatal dysmyelinating disease. Consistent with its role in supplying acetate for myelin lipid synthesis, ASPA is thought to be cytoplasmic. Here we describe the occurrence of ASPA within nuclei of rat brain and kidney, and in cultured rodent oligodendrocytes. Immunohistochemistry showed cytoplasmic and nuclear ASPA staining, the specificity of which was demonstrated by its absence from tissues of the *Tremor* rat, an ASPA-null mutant. Subcellular fractionation analysis revealed low enzyme activity against NAA in nuclear fractions from normal rats. Whereas two recent reports have indicated that ASPA exists as a dimer, size-exclusion chromatography of subcellular fractions showed ASPA is an active monomer in both subcellular fractions. Western blotting detected ASPA as a single 38 kD band. Because ASPA is small enough to passively diffuse into the nucleus, we constructed, expressed, and detected in COS-7 cells a green fluorescent protein-human ASPA (GFP-hASPA) fusion protein larger than the permissible size for the nuclear pore complex. GFP-hASPA was enzymatically active and showed mixed nuclear-cytoplasmic distribution. We conclude that ASPA is a regulated nuclear-cytoplasmic protein that may have distinct functional roles in the two cellular compartments.—Hershfield, J. R., Madhavarao, C. N., Moffett, J. R., Benjamins, J. A., Garbern, J. Y., Namboodiri, A. Aspartoacylase is a regulated nuclear-cytoplasmic enzyme. *FASEB J.* 20, E1482–E1494 (2006)**

Key Words: Canavan Disease · N-acetylaspartate · aminoacylase · kidney · oligodendrocytes · Tremor *rat*

MUTATIONS IN THE gene encoding aspartoacylase (ASPA, EC 3.5.1.15), which catalyzes deacetylation of *N*-acetyl-aspartate (NAA), result in Canavan Disease (CD), a neurodegenerative disorder most prevalent among Ashkenazi Jews. The pathology of CD is marked by brain vacuolization and dysmyelination, resulting in death during childhood (1, 2). Considerable effort has been devoted to understanding the basis of CD by elucidating the function of ASPA in the CNS. Developmental increases in ASPA and NAA correlate with myelination (3–8) and several studies have shown incorporation of acetate from NAA into myelin lipids (9–13). Overall acetate levels and lipid synthesis have recently been shown to be deficient in brains of CD knockout mice (14), providing strong support for the hypothesis that NAA in the CNS supplies acetyl groups for lipid synthesis during myelination (3, 7, 14). The functions served by ASPA in other tissues such as kidney (17) are currently unknown.

ASPA activity was originally found to be restricted to cultured oligodendrocytes (15). Subsequently, antibodies against recombinant human ASPA (8) and recombinant murine ASPA (16) demonstrated ASPA expression primarily in oligodendrocytes in rat brain by immunohistochemistry. These and earlier studies showing ASPA activity restricted to the cytoplasm (6, 7) and in membrane fractions (11, 17, 18) have implied a specific subcellular localization for ASPA, but this remains to be established definitively. Immunohistochemistry of rat brain sections identified oligodendrocytes expressing ASPA protein and provided initial indications that ASPA is present in the nucleus as well (16). Currently, all hypotheses linking the basis of CD pathology to the function of ASPA refer to a cytoplasmic role for the enzyme. However, in order to completely understand and fully treat the disease, the possibility of nuclear ASPA localization, and the concomitant possibility of specific nuclear functions, warrant investigation.

Recently, separate analyses have suggested that recombinant human ASPA [MW of 35–38 kD (19)] exists as a dimer without posttranslational modifications (8, 19, 20). ASPA purified from *E. coli* was initially characterized as a dimer by mass spectroscopy (20) and later by Western blot (8), implying covalent dimerization. However, neither study investigated whether ASPA is active as a dimer, or whether the dimer band was ASPA-specific.

[1]Correspondence: Dept. of Anatomy Physiology and Genetics, USUHS, 4301 Jones Bridge Rd, Bethesda, MD 20814 USA. E-mail: anamboodiri@usuhs.mil

doi: 10.1096/fj.05-5358fje

0892-6638/06/0020-1482 © FASEB

In this report we investigated ASPA's subcellular localization using rat organs, cultured oligodendrocytes, and transfected cells. Furthermore, we explored the catalytic properties of ASPA in subcellular fractions from rat brain and kidney.

MATERIALS AND METHODS

Rodent oligodendrocyte culture

Primary rat oligodendroglia were cultured from brains of 2 d old Sprague-Dawley rat pups as described previously (21). Maturity was determined by using antibodies against cell type-specific markers (21); specifically, expression of myelin oligodendrocyte glycoprotein (MOG; detected with monoclonal antibody (mAb) 8–18C5; hybridoma cells) (22) was associated with full maturity.

Enriched murine oligodendroglia cultures were prepared from brains of 1 to 2 d-old Balb/C mice (23) by a modification of the shake-off method (24). To improve oligodendrocyte survival, enriched oligodendrocyte cultures were maintained in a 2:1 mixture of (*i*) chemically defined medium with 2% newborn calf serum and (*ii*) astrocyte conditioned medium consisting of Dulbecco's modified Eagle's medium (DMEM) with 10% newborn calf serum. Three days later, fluorodeoxyuridine (5 μg/ml) was added to inhibit proliferation of astrocyte and other cellular contaminants. Cells were analyzed 5–9 d after enrichment and typically contained ~90–95% oligodendrocytes, most of which were mature and positive for MBP and PLP1 staining, as described previously (23).

Aspartoacylase immunocytochemistry

Cultured rat oligodendroglia were fixed with 4% paraformaldehyde (10 min), washed with PBS, and incubated overnight (4°C) with a monoclonal anti-MOG antibody (Ab) (22) (diluted 1:5 in PBS and 3% BSA, BSA) and a polyclonal antibody (pAb) against full-length recombinant murine ASPA (αASPA, diluted 1:500 in PBS). Cells were washed with PBS, preincubated with 5% donkey serum (20 min), and incubated with FITC-conjugated donkey anti mouse (1:200) and Cy3-conjugated donkey anti-rabbit (1:400) secondary antibodies diluted in PBS + 3% BSA (1 h, RT). Cells were washed with PBS and mounted using Vectashield medium with 4′,6′-diam idino-2-phenylidole (DAPI) (Vector Lab, Burlingame, CA).

Briefly, immunocytochemistry on cultured murine oligodendrocytes was performed with a 1:5000 dilution of rabbit sera against a domain conserved in rodent and human ASPA (residues 83–101 SEDLPYEVRRAQEINHLFG; pepASPA) after treating the cells with 0.01% Triton-X. Bound Ab was detected using appropriate fluorescently labeled anti-rabbit IgG. Indirect epifluorescent microscopy was performed using a Nikon TE2000 instrument (Melville, NY).

COS-7 cells were fixed (20 min in 10% formalin) 30–48 h posttransfection, washed with PBS, and incubated 1 h with 1:1000 αASPA or pepASPA in PBS plus 3% BSA. Following PBS washes, cells were incubated 1 h in 1:100 FITC-conjugated goat anti-rabbit secondary Ab (Jackson, West Grove, PA), washed, and mounted on slides using VectaShield Mounting Medium with DAPI. Confocal microscopy and subsequent data analysis were done using the Zeiss Pascal Laser Scanning Confocal Microscope and proprietary software (Thornwood, NY).

Aspartoacylase immunohistochemistry

Confocal microscopy was performed as described above. Peroxidase immunohistochemistry was performed as described previously (16). Briefly, free-floating rat tissue sections were blocked by incubation for 20 min in PBS containing 2% NGS and 0.1% sodium azide. Endogenous peroxidase was blocked by washing sections in PBS and incubating them in a 50:50 mixture of methanol and water containing 1% H_2O_2 for 30 min with agitation. Sections were incubated with 1:5000 crude αASPA for 24 to 48 h at room temperature, with constant rotary agitation. Bound antibodies were visualized by the avidin-biotin complex (ABC) method with horseradish peroxidase as the enzyme marker (Vectastain Elite, Vector) and developed with a Ni and Co enhanced diaminobenzidene chromogen (Pierce, Rockford, IL). Sections were mounted on slides with resin, and images were acquired with an Olympus BX51 microscope and Qcolor5 digital camera.

Subcellular fractionation

Rat brains and kidneys were removed from adult Sprague-Dawley male and female rats, frozen on dry ice, and stored at −80°C until use. All steps were performed on ice. Tissues were minced and homogenates were prepared by 8–10 low-speed up/down strokes with a Potter-Elvejham homogenizer in nuclear isolation medium (NIM; 0.25 M sucrose; 25 mM KCl; 5 mM $MgCl_2$; 10 mM Tris-HCl, pH 7.4) supplemented with protease inhibitor cocktail (15 μl/mL) and phosphatase inhibitors (4.52 nM microcystin-LR, 20 μM (-)-p-bromotetramisole oxalate, 4.59 μM cantharadin, 2 mM imidazole, 4.84 mM sodium tartrate, 1.17 mM sodium molybdate, 1 mM sodium orthovanadate) (Sigma, St. Louis, MO). Following passage through cheesecloth, filtrates were centrifuged (800 g, 10 min, 4°C), resuspended in NIM, and recentrifuged.

A) Resulting supernatants were adjusted to "homogenization buffer" (*HB*; 0.5 mM DTT; 50 mM Tris-HCl, pH 8.0; 50 mM NaCl; 0.05% IGEPAL CA-630; 8% glycerol). Supernatant resulting from the second centrifugation (16,000 *g*, 20 min, 4°C) was used in subsequent analysis as cytoplasmic protein extract.

B) Resulting crude nuclear pellets were resuspended in highly viscous NIM (containing 2.3 M sucrose) and pelleted by swinging bucket rotor ultracentrifugation (100,000 *g*, 80 min, 4°C). An aliquot of the resulting purified nuclei was resuspended in NIM and stained with DAPI to observe characteristic nuclear morphology. Remaining nuclei were resuspended in HB, sonicated, and repelleted (16,000 *g*, 10 min, 4°C). Resulting supernatant was used as nuclear protein extract for subsequent analysis.

Protein concentrations were determined by Bio-Rad's DC protein assay (Hercules, CA) based on the method of Lowry. Cytoplasmic contamination of nuclear extract was assessed by using a commercial lactate dehydrogenase (LDH) assay (Randox, Oceanside, CA).

Anion exchange chromatography

Macroprep diethylaminoethyl (DEAE) weak cellulose resin (Bio-Rad) was used as an anion-exchange matrix to separate ASPA from the bulk of cytoplasmic and nuclear proteins, respectively. Resin (2.5 μl bed vol) was equilibrated with 10 column vol of HB before being mixed gently (1 h, 4°C) with 8.5 μl of sample (33 mg protein). Three unbound fractions were collected immediately, and excess unbound proteins were washed with 10 column vol of HB. Proteins were then eluted by 6 column vol washes of HB containing (*i*) 150 mM NaCl, (*ii*) 250 mM NaCl, and (*iii*) 500 mM NaCl. Fractions

were concentrated, assayed for protein, and analyzed for ASPA activity and content by spectrophotometric (cytoplasmic extract) or radiometric (nuclear extract) assay, as well as by Western blot. Maximal activity was identified in fractions 1 and 2 under 150 mM NaCl elution for cytoplasmic extract. Anion exchange chromatography was performed three times using separate nuclear and cytoplasmic preparations.

Size-exclusion chromatography

The column (TOSOHAAS G3000SW, Thompson, Clear Brook, VA) was equilibrated in HB minus DTT, and a standard curve was prepared using protein standards [ribonuclease A, chymotrypsinogen, carbonic anhydrase, ovalbumin, BSA, alcohol dehydrogenase (ADH), β-amylase (Sigma)]. A 0.5 μl aliquot of anion-exchange chromatography sample was injected into the column and eluted at 0.5 μl/min and collected as ~45 × 0.5 μl fractions. For some experiments, multiple injections resulted in pooled fractions. Fractions were concentrated, assayed for protein, and analyzed for ASPA activity and content by radiometric assay and Western blot.

Aspartoacylase enzyme assays

A coupled spectrophotometric ASPA activity assay based on β-NADH oxidation of ASPA-liberated aspartate (25) was followed as described elsewhere (26). A high-sensitivity radiometric assay involving thin-layer chromatography (TLC)-based product separation and phosphor image-based quantification was followed as described previously (26).

SDS-PAGE and Western blot

Samples were diluted in 5× loading buffer (Quality Biological, Gaithersburg, MD), reduced with 10 mM DTT, and heated (90°C, 5 min) prior to loading onto 10% precast Tris-Glycine gels (Invitrogen, Carlsbad, CA). Following electrophoresis, samples were transferred to Immobilon-P PVDF (Millipore, Bedford, MA) membranes using the XCell II blotting module (Invitrogen). Membranes were blocked (PBS, 0.05% v/v Tween-20, and 5% NGS) for 1 h at room temperature, followed by overnight 4°C incubation with αASPA, pepASPA, monoclonal green fluorescent protein (GFP) Ab (Chemicon, Temecula, CA), or monoclonal β-tubulin Ab (Upstate, Charlottesville, VA). Following brief washing, horseradish peroxidase-conjugated goat anti-rabbit or antimouse secondary Ab was added at dilutions of 1:2500–1:5000. Membranes were washed and developed in Super Fast diaminobenzidine substrate (Sigma).

Plasmid constructs

Full-length human ASPA cDNA was subcloned by polymerase chain reaction (PCR) using primers ATGACTTCTTGTCACATTGCT (forward) and CTAATGTAAACAGCAGCGAAT (reverse) from pBAD/Thio-TOPO (Invitrogen) (27) into the TOPO-T/A cloning site of pcDNA3.1/NT-GFP-TOPO. The resulting GFP-hASPA plasmid expresses a fusion protein of cycle 3 GFP fused to the NH_2 terminus of ASPA. Full-length human ASPA cDNA was also subcloned into the TOPO-T/A cloning site of pcDNA3.1/V5-His-TOPO such that the resulting hASPA plasmid expresses untagged, native ASPA. Control plasmids expressing GFP alone and GFP fused to tandem nuclear localization signals (NLS) of SV40 Large T Antigen (nuc-GFP) were obtained from Invitrogen.

Cell culture and transient transfections

COS-7 (American Type Culture Collection, Manassas, VA) cells were grown at 37°C with 5% CO_2, cultured in DMEM containing 10% FBS, grown to confluence, and subcultured every 3–4 d. Transient transfections were performed using Lipofectamine 2000 (Invitrogen). For fluorescence microscopy, 0.8 μg DNA was added to cells grown on coverslips in 24-well plates. For Western blot and enzyme activity analyses, 8 μg DNA was added to cells in 60 mm culture dishes. Transfected COS-7 cells were harvested 24–48 h posttransfection by treatment with 2 mM EDTA (15 min, 37°C), spun down, and washed with PBS. Whole cell extracts were generated by sonicating cell pellets in HB. Cellular debris was then removed (16,000 *g*, 10 min, 4°C), and protein concentrations were determined.

Statistical analysis

Enzyme activities are presented as means ± SEM. Differences between groups were analyzed by *t* test for a significance level of $P < 0.05$.

RESULTS

Subcellular localization of ASPA in rodent oligodendrocytes

We recently reported ASPA staining throughout oligodendrocytes in rat brain sections by immunohistochemistry (16). These studies also raised the possibility that ASPA might be expressed in the nucleus as well as the cytoplasm of oligodendrocytes. In the absence of an obvious functional role for ASPA in the nucleus, we have thoroughly examined the occurrence of nuclear ASPA using multiple techniques. Two online subcellular localization prediction programs, LOCTree and PSORTII (http://psort.nibb.ac.jp), based on amino acid sequence, predict that human ASPA is partially nuclear (34.8% cytoplasmic and 17.4% nuclear).

Indirect immunofluorescence of cultured primary rat and mouse oligodendrocytes enabled us to show ASPA merged with DAPI, a DNA stain, in representative cells (**Fig. 1**). Our previous experiment used a pAb against full-length recombinant murine ASPA (αASPA) (16). In Fig. 1*B* we utilized newly generated rabbit serum against a conserved ASPA peptide (pepASPA) to substantiate Ab specificity for ASPA in the nucleus. Among cell types of the CNS, ASPA expression and activity have been found primarily in oligodendrocytes (4, 7, 15, 16). We confirm here that ASPA is highly expressed in mature oligodendrocytes by using a maturity-specific Ab raised against myelin oligodendrocyte glycoprotein (MOG) (see Fig. 1*A*) as well as CC1 (see Fig. 1*B*). Note that in Fig. 1*A*, weak ASPA staining appears in several cells that do not stain positively for MOG. In this representative mature oligodendrocyte cultured from rat brain, MOG was confined to the peripheral cytoplasm and cell processes, while ASPA stained throughout cytoplasm and the nucleus (Fig. 1*A*). This phenomenon was confirmed in murine oli-

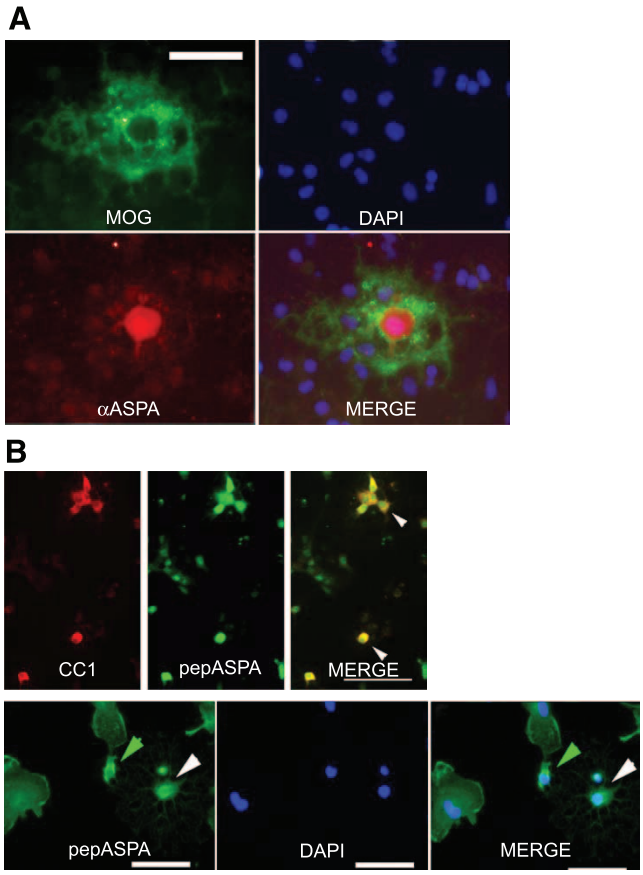

Figure 1. ASPA in cultured oligodendrocytes. *A)* ASPA staining in a representative mature cultured rat oligodendrocyte using an Ab against recombinant murine ASPA (αASPA) (red). Cell processes are highlighted using an Ab against myelin oligodendrocyte protein (MOG) (green). Nuclei are stained with DAPI (blue). Merged field shows ASPA colocalizes with DAPI. Scale bar = 20 μm. *B)* ASPA staining in cultured murine oligodendrocytes using serum against a conserved ASPA peptide (pepASPA) (green). Nuclei are stained with DAPI (blue). Cytoplasm is stained with CC1 oligodendrocyte marker protein (red). *Top panel)* White arrows point to examples of cells where CC1 and ASPA staining correlate very weakly. *Bottom panel)* Perinuclear staining examples in mostly differentiated oligodendrocytes are depicted with green arrows. An example of predominantly nuclear ASPA staining is marked by a white arrow. Merged field shows ASPA colocalizing with DAPI. *Top panel)* scale bar = 100 μm. *Bottom panel)* Scale bar = 20 μm.

godendrocytes using staining for CC1 marker protein (see Fig. 1*B*, top panel). ASPA staining that does not colocalize with cytoplasmic CC1 can be described as nuclear by colocalization with DAPI (Fig. 1*B*, bottom panel).

To address whether ASPA staining observed in Fig. 1 represented true nuclear localization rather than cytoplasmic overlay, Z-series were generated by confocal microscopy, capturing multiple depths of a rat brain section stained with αASPA. The first representative panel (**Fig. 2*A***) shows several examples of ASPA and DAPI colocalization, indicative of nuclear ASPA in rat brain oligodendrocytes. Furthermore, ASPA colocalized with DAPI in the same planes, indicating that fluorescence due to ASPA arises from within the nucleus. ASPA in these oligodendrocytes was both cytoplasmic and nuclear. Additionally, morphometric data show that the area of ASPA staining is larger than, and includes, the area stained for DAPI (nucleus) at several depths of the Z-series (Fig. 2*C*). Thus, it is highly suggestive of ASPA localization in both cytoplasm and nucleus. Also, cells within the same tissue section showed ASPA in the cytoplasm only, as confirmed by cross-sectional depth analysis in the Z-plane (Fig. 2*B*). Our results indicate that ASPA can be found in three distinct configurations within oligodendrocytes: predominantly nuclear, mixed nuclear-cytoplasmic, and predominantly cytoplasmic.

ASPA staining is absent throughout *Tremor* rat brain sections

The *Tremor* rat is a mutant epilepsy model that was found to lack the entire ASPA gene (28, 29). Because ASPA is completely absent in this strain, as opposed to a truncated form in the knockout mouse for CD (30), and because we have consistently analyzed rats (not mice) for NAA and ASPA (3, 7, 16, 31), we used *Tremor* rats as ASPA −/− model systems. We compared wild-type (WT) and *Tremor* rat brain sections by peroxidase immunohistochemistry with αASPA to assess whether nuclear ASPA staining was based on the ASPA gene (**Fig. 3**). As reported previously (16), ASPA protein was found in oligodendrocytes throughout the CNS. Figure 3*A* shows ASPA expression in three brain regions—cortex, corpus callosum, and striatum. ASPA-expressing oligodendrocytes were heavily concentrated in white matter of the corpus callosum, as previously shown (3, 4). In corresponding *Tremor* rat tissue sections, using the same concentration of primary Ab, ASPA staining was completely absent (Fig. 3*B*). Since αASPA displayed no cross-reactivity with antigens in the *Tremor* rat brain, the observed nuclear localization must also be due to ASPA gene product.

Localization of ASPA in rat kidney

Although ASPA was originally purified from hog kidney (32), its cellular localization within this organ has yet to be examined. Peroxidase immunohistochemistry of rat kidney sections in **Fig. 4** shows abundant ASPA expression in kidney. ASPA was selectively localized to kidney cortex and absent from medulla (Fig. 4*A*). Within kidney cortex, ASPA was strongly expressed in proximal tubule cells but was absent from glomeruli (Fig. 4*C*). Using *Tremor* rat kidney sections, again we observed that αASPA did not cross-react with other antigens, indicating that immunoreactivity was selectively localizing ASPA gene product (Fig. 4*D*). At higher magnification in kidney cortex from WT rats, heavy nuclear staining was observed in individual proximal tubule cells (Fig. 4*B*).

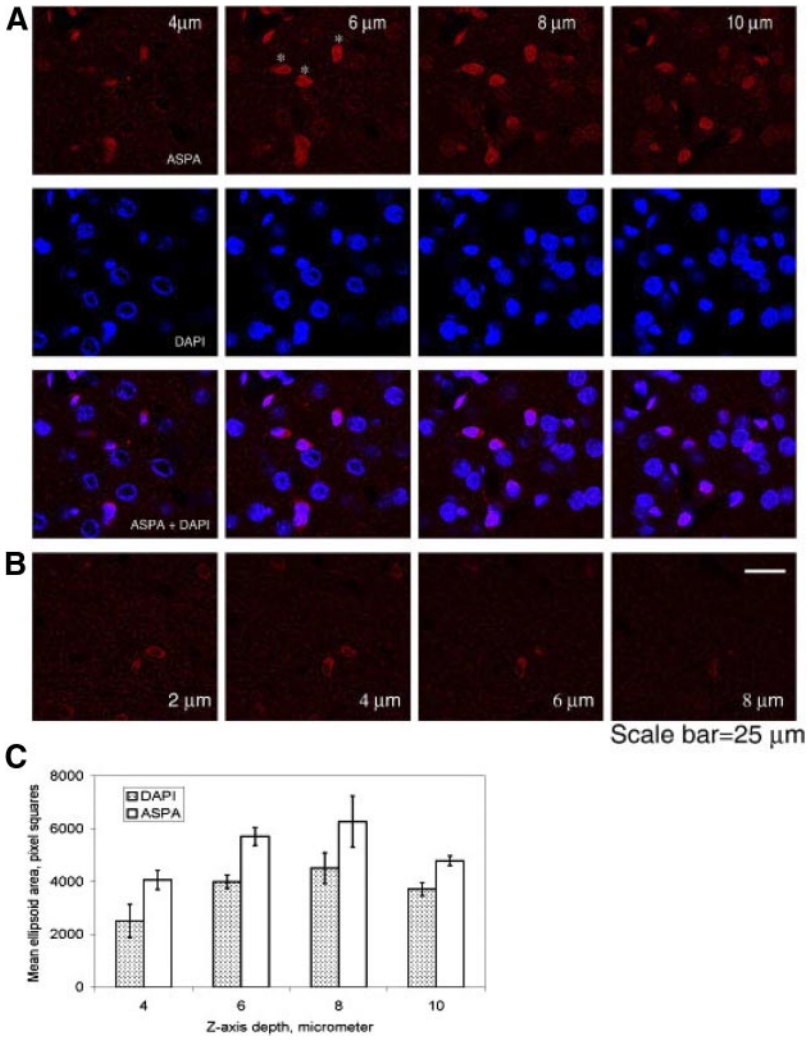

Figure 2. Subcellular localization of ASPA in rat brain sections. *A)* Z-series generated by confocal microscopy capturing multiple depths of a rat brain section stained with αASPA. Examples of predominantly nuclear ASPA (red) colocalizing with DAPI at same depths are shown. *B)* ASPA can also be strictly cytoplasmic. Scale bar = 25 μm. *C)* Cellular morphometric data for ASPA and DAPI staining. The areas corresponding to ASPA (red) and DAPI (blue) were calculated by approximating to an ellipsoid. The exact number of pixels of the long axis and short axis of the ellipse were obtained using Adobe Illustrator software on the raw digital images. Three cells were chosen (identified with asterisks) and compared for the areas of ASPA and DAPI using *t* test with equal variances. Comparisons were made depth-wise (three values), as well as across all depths for each cell (four values); ASPA areas were significantly larger than DAPI areas by at least 500 pixel squares at all the depths and for every cell ($P < 0.05$).

Nuclear ASPA is catalytically active

Nuclei isolated from adult rat organs by sucrose density gradient ultracentrifugation, when resuspended in nonlytic buffer and stained for DNA by DAPI, were plentiful and intact (data not shown). Furthermore, LDH, a cytoplasmic marker, showed specific activity in the nuclear extract that was virtually negligible compared with cytoplasmic extract (~2%).

We utilized a highly sensitive radiometric ASPA assay (26) to analyze subcellular fractions for enzyme activity. For comparison, we analyzed cytoplasmic extracts (**Fig. 5*A***) from kidney and brain of WT and ASPA −/− mutant *Tremor* rats (28). As described previously, there was ~10-fold higher activity in kidney than in brain (6, 17, 30). This activity was due to the ASPA gene as it was not present in *Tremor* rat tissue extracts. We then assayed nuclear extracts (Fig. 5*B*) and noted a similar ratio of elevated kidney-to-brain ASPA activity (~6:1 in cytoplasm, ~3:1 in nucleus). Nuclear ASPA activity was undetectable in *Tremor* rat tissues, confirming it was due to ASPA gene product in WT rats. The percentage of nuclear ASPA activity against NAA substrate relative to

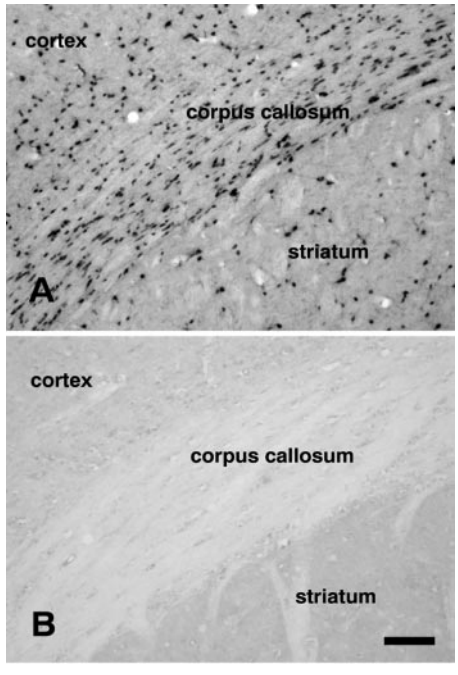

Figure 3. ASPA localization in rat brain sections. *A)* ASPA immunoreactivity in the corpus callosum and adjacent structures of WT rats. *B)* Staining is completely absent from ASPA null *Tremor* rat tissue sections. Scale bar = 120 μm.

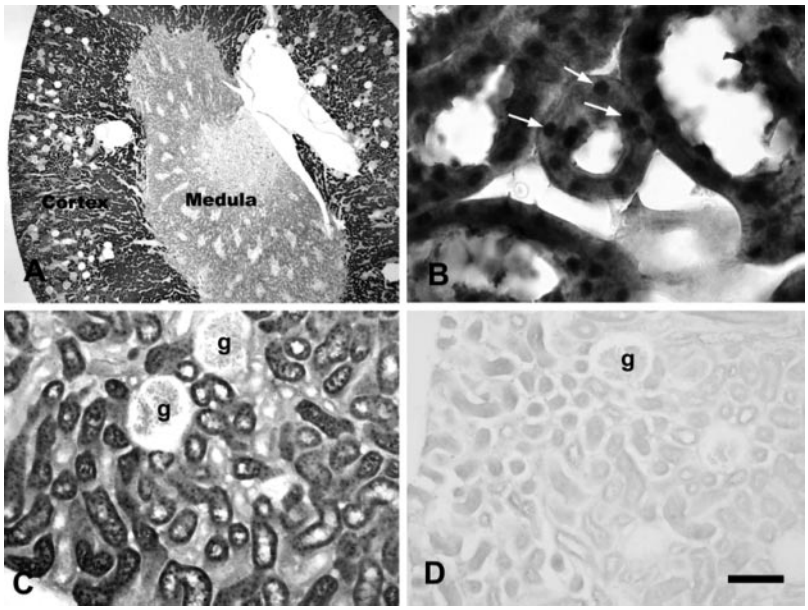

Figure 4. ASPA localization in rat kidney sections. *A)* ASPA expression was strong in kidney cortex, but was low in the medulla. *B)* ASPA expression was exceptionally strong in the nuclei of some proximal tubule cells in the cortex. White arrows point to representative nuclei. *C)* ASPA was expressed throughout proximal tubules but was not observed in glomeruli in WT rat kidney cortex (g in panel *C*). *D)* ASPA immunoreactivity was absent from ASPA-null *Tremor* rat kidney sections. Scale bar = 800 μm (*A*), 50 μm (*B*), 200 μm (*C, D*).

cytoplasmic activity was ~3% in kidney and ~6% in brain extracts.

To qualitatively analyze what proportion of ASPA protein existed in our nuclear extracts, we analyzed kidney extracts by Western blot using both αASPA and pepASPA antibodies (Fig. 5*C*). Previous immunoblotting studies using different ASPA antibodies have identified an ASPA monomer and a putative ASPA dimer (8, 20). The present study is the first to immunoblot ASPA from kidney, where two other aminoacylases exist in great abundance. Therefore, we relied on the *Tremor* rat to determine which band detected by our polyclonal antibodies actually reflected ASPA protein. Both antibodies detected an ASPA monomer band at 38 kD that was missing from *Tremor* rat extract (Fig. 5*C*). This ASPA monomer was detected in nuclear extract at a considerably lower level than in cytoplasmic extract, comparable to its correspondingly lower activity. Thus, it appears that only a small population of ASPA is in the nucleus. Each Ab cross-reacted with some other proteins from *Tremor* rat extracts (see "Mut" lanes). The prominent band detected at 32 kD likely reflects aminoacylase III, which has been characterized as a 32–35 kD protein (33, 34). Consistent with the cytoplasmic localization of both aminoacylase I (35) and aminoacylase III (33), these cross-reacting bands were not detected in our nuclear extracts (Fig. 5*C*). This lack of cross-reactive cytoplasmic bands carrying over from cytoplasmic to nuclear preparations indicates the ASPA monomer band in nuclear extract was not the result of cytoplasmic contamination. Additionally, this supports the observation that low nuclear activity in kidney and brain extracts is not due to cytoplasmic contamination. The putative ASPA dimer band detected by Western blotting of rat brain homogenates using serum against recombinant human ASPA (8) also appeared in our immunoblots of *Tremor* rat extracts (Fig. 5*C*), as well as in WT rat cytoplasmic extract following incubation with αASPA that was pretreated with its antigen (data not shown), indicating that this band was the result of cross-reactivity rather than dimerization.

Nuclear ASPA displays weaker ionic behavior than cytoplasmic ASPA

To assess the biochemical nature of ASPA within cytoplasm and within nuclei, we partially purified ASPA from each extract and compared column elution properties. ASPA-rich kidney tissue (see Fig. 5) was used as the enzyme source. Our purification plan involved (*i*) anion-exchange chromatography and (*ii*) HPLC size-exclusion chromatography. The methods were each tested separately using crude solubilized enzyme (data not shown) and subsequently combined in the order presented.

DEAE cellulose chromatography was used as the first chromatographic step for enzyme purification; ASPA activity profiles are presented in **Fig. 6**. Elution with 150 mM NaCl was used to recover maximum enzyme activity, rather than 75 mM NaCl elution used for ASPA purification from bovine brain (18). We tested NaCl concentrations up to 1 M in assay buffer and found no effect on ASPA activity in crude rat kidney homogenate (data not shown). For cytoplasmic extracts (Fig. 6*A*), as much as 70% of the enzyme activity was bound to the column and eluted with 150 mM NaCl medium. The remaining ~30% of activity was found in the unbound fraction. ASPA activity was not detected in subsequent elutions with 250 mM and 500 mM NaCl for either extract (data not shown). There was a statistically significant ~6-fold enrichment of ASPA-specific activity in the 150 mM NaCl vs. the unbound fraction (from 250 nmol/h/mg protein to 1500 nmol/h/mg protein). For nuclear extracts (Fig. 6*B*), less than 50% of total

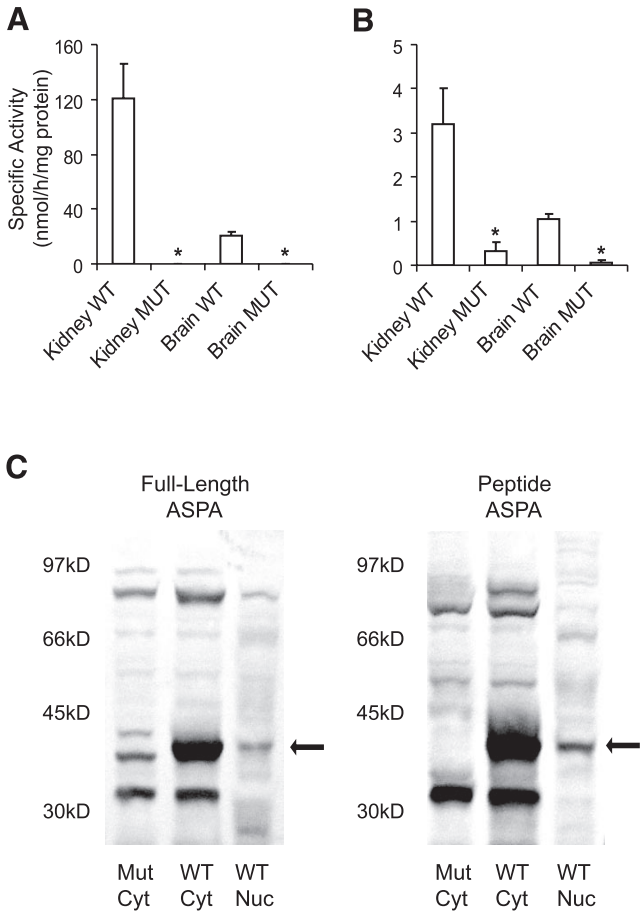

Figure 5. ASPA in cytoplasmic and nuclear extracts. Subcellular fractionation and radiometric enzyme assay are described in Materials and Methods. Specific activities are presented as mean ± SEM for three to four data points. *A)* ASPA activity detected in rat kidney and brain cytoplasmic protein extracts is completely absent in ASPA null *Tremor* rat (MUT) tissues. *B)* ASPA activity detected in rat kidney and brain sucrose density gradient-purified nuclear protein extracts is virtually absent in *Tremor* rat tissues. (*Indicates mutant values differ significantly from WT values, $P < 0.05$). *C)* Western blot of ASPA from fractionated kidney extract. *Left panel)* Western blot (1:2000) with αASPA. *Right panel)* Western blot (1:2000) with pepASPA. *Mut Cyt, Tremor* rat (mutant) cytoplasmic extract. *WT Cyt,* WT cytoplasmic extract. *WT Nuc,* WT nuclear extract. 100 μg protein per lane. Arrows point to the ASPA monomer, which is absent from *Tremor* rat extract.

enzyme activity was bound to the column and eluted with 150 mM NaCl buffer. There was virtually no enrichment of nuclear ASPA specific activity under the described conditions.

Active rat kidney ASPA is a monomer

The first two 150 mM fractions ("150mM" in Fig. 6) containing the majority of cytoplasmic enzyme activity were pooled and concentrated for further purification by size-exclusion chromatography. For comparative purposes, corresponding 150 mM fractions were similarly pooled and concentrated for the nuclear extract. **Figure 7** shows ASPA elution profiles from HPLC size-exclusion chromatography. To avoid a clumping effect whereby highly concentrated sample resulted in ASPA activity detected both at very high sizes (>300 kD) as well as at a size corresponding to the ASPA monomer (data not shown), a relatively dilute cytoplasmic sample from the 150 mM NaCl DEAE-cellulose elution was separated by gel filtration. Maximum specific and total activities were observed in a size range (between 29 and 43 kD) containing the ASPA monomer (Fig. 7*A*). The MW values calculated from a log plot using MW standard proteins corresponded well (35–38 kD) to the size of the ASPA monomer (data not shown). Nuclear protein samples were found to follow a similar pattern, with peak activity corresponding to the ASPA monomer (Fig. 7*B*). In nuclear extract only, there appeared to be residual activity (~25% peak activity) corresponding to a MW of 67–200 kD, which could reflect a reduced activity corresponding to putative dimerized ASPA (8, 20). This activity might have also existed in the cytoplasmic extract at a low level, undetectable due to the tailing effect from high activity of the monomer.

Maximum total activities recovered from ~450 rat kidneys following two rounds of purification were 236 nmol/h for cytoplasmic ASPA and 8.3 nmol/h for nuclear ASPA, respectively, indicating that only a very small proportion of ASPA activity against NAA (3%) is found in kidney nuclei. However, purification sufficiently enriched the specific activity of nuclear ASPA so that it was higher than that of the initial rat kidney cytoplasmic extract: 185 nmol/h/mg protein vs. ~121

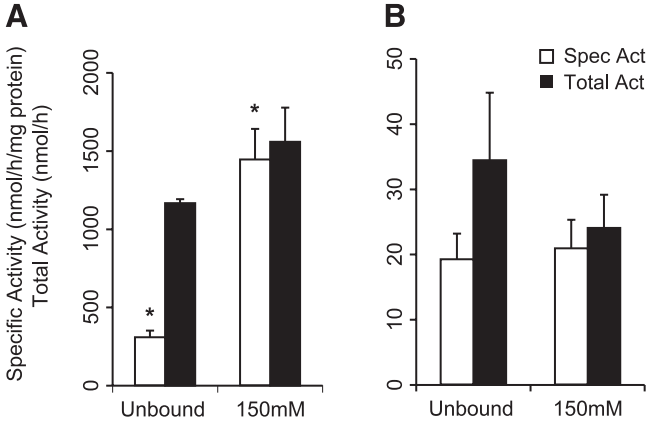

Figure 6. Anion-exchange chromatography ASPA activity elution profiles from rat kidney nuclear and cytoplasmic extracts. Column setup and NaCl elution gradient, as well as spectrophotometric (cytoplasmic extract) and radiometric (nuclear extract) enzyme assays, are described in Materials and Methods. Each fraction represents two pooled fractions with average specific activities and summed total activities. Data are presented as mean ± SEM for three points. *A)* For cytoplasmic extract, specific activity of 150 mM fractions is significantly higher ($*P < 0.05$) than that of unbound fractions. Total activity of the 150 mM fractions is also elevated compared to unbound fractions. *B)* For nuclear extract, both specific and total activities are nearly evenly distributed between unbound and 150 mM fractions. No activity was found for cytoplasmic and nuclear extracts with 250 mM and 500 mM NaCl elutions (data not shown).

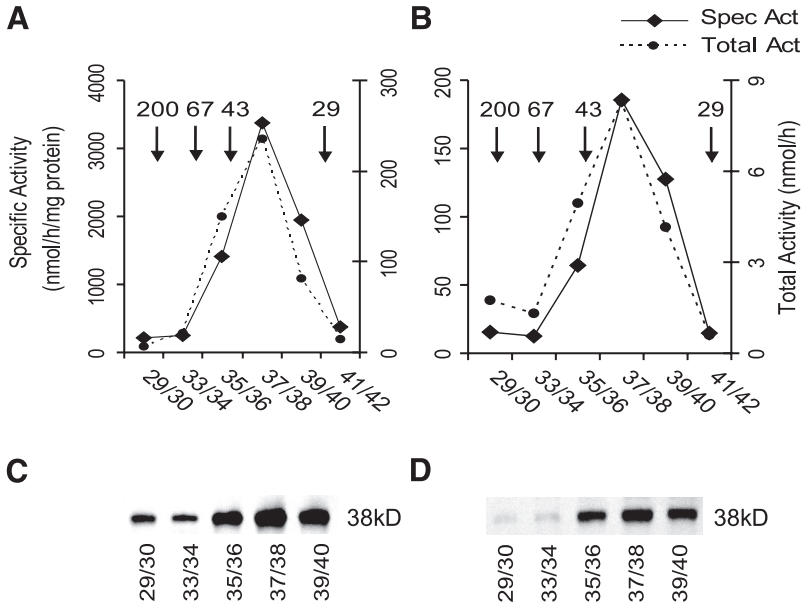

Figure 7. Determining the size of active rat kidney nuclear and cytoplasmic ASPA. Pooled 150 mM NaCl anion-exchange chromatographed fractions were concentrated and injected into a size-exclusion column. Adjacent fractions corresponding to 500 μl/min elution were pooled and concentrated. *A–B)* Radiometric enzyme assay is described in Materials and Methods. The data are averages of two assays. Peak specific and total ASPA activity from both cytoplasmic (*A*) and nuclear (*B*) 150 mM NaCl anion-exchange fractions occur between fractions 36 and 40, corresponding to a MW of 38 kD as determined by standard curve (data not shown). Sizes (in kDa) of MW marker proteins are indicated by arrows. *C)* Western blot (1:2000 αASPA) of cytoplasmic protein (2.5 μg per lane) in size-exclusion chromatography fractions. *D)* Western blot (1:1000 αASPA) of nuclear protein (8 μg per lane) in size-exclusion chromatography fractions.

nmol/h/mg protein. Western blot analysis of size-exclusion fractions complemented both activity elution profiles. The ASPA monomer band was present in all cytoplasmic fractions, with peak intensity in fractions with maximal activity (Fig. 7*C*). In contrast, the ASPA monomer band was present only in nuclear fractions where ASPA activity was present, rather than throughout the entire elution (Fig. 7*D*). Careful inspection of the *y*-axes for both extracts reveals relatively significant residual activity in fractions corresponding to high MW in cytoplasmic but not nuclear extract, which accounts for the weak ASPA bands in these cytoplasmic fractions.

Generation and confirmation of GFP-hASPA

ASPA is small enough to passively diffuse through the nuclear pore complex (NPC). Therefore, we tagged ASPA with GFP so the size of the fusion protein would exceed the 40–60 kD size cutoff for passive diffusion through the NPC (36). GFP was linked to the NH_2 terminus of ASPA (GFP-hASPA) because ASPA's catalytic domain has been tentatively assigned toward its C-terminus (19, 37, 38) and because linking GFP to either terminus of a protein tends to result in identical subcellular distributions (39, 40). Immunoblots of transiently transfected COS-7 cells confirmed that additional linker residues connecting cycle 3 GFP (27 kD) to the hASPA (38 kD) increased the size of GFP-hASPA to 69 kD (**Fig. *8A***). Western blots of control transfections with GFP alone and native hASPA confirmed their respective individual sizes. As previously reported for other kidney cell lines (8, 20, 38), ASPA was not endogenous to COS-7 cells, allowing us to discern ASPA from background bands at ~50 and ~80 kD ("No DNA" lane in Fig. 8*A*). GFP-hASPA was found to be catalytically active similar to native untagged hASPA (Fig. 8*B*), implying it is useful for studying ASPA's subcellular localization. ASPA activity was undetectable in control GFP and mock transfections.

Subcellular localization of transfected ASPA

The distribution of transiently transfected GFP-hASPA in formalin-fixed COS-7 cells was mostly mixed nuclear-cytoplasmic (see **Fig. 9*A***, "GFP-hASPA"). GFP alone demonstrated mixed nuclear-cytoplasmic fluorescence characteristic of a small, diffuse protein while nuc-GFP (see Materials and Methods) demonstrated predominantly nuclear fluorescence (Fig. 9*A*). The ratio of nuclear to cytoplasmic GFP-hASPA was determined by merging GFP and DAPI images from several fields of transfected COS-7 cells to assess the extent of nuclear, mixed, and cytoplasmic staining. GFP-hASPA's distribution (Fig. 9*B*) was very similar to that predicted for ASPA obtained using PSORTII (http://psort.nibb.ac.jp): 17.4% nuclear and 34.8% cytoplasmic. Finally, we used indirect immunofluorescence with pepASPA and a FITC-conjugated secondary Ab to analyze the subcellular distribution of transfected native hASPA. In Fig. 9*C* we verified that native ASPA is also a mixed nuclear-cytoplasmic protein, as visualized at high magnification by merger with DAPI images.

DISCUSSION

For many years ASPA has been assumed to be a soluble, cytoplasmic enzyme with some partial membrane association (6, 11, 17, 18). However, our recent immunohistochemical localization study raised the possibility that ASPA may also be found in the nucleus of oligodendrocytes (16). In our current report we explored this possibility and have established that ASPA is a nuclear-cytoplasmic enzyme. The occurrence of ASPA in the nucleus was demonstrated using immunofluorescence, confocal microscopy, peroxidase immunohistochemistry, and immunoblotting. Additionally, we have shown that ASPA in the nucleus of rat kidney and brain cells retains low levels of catalytic activity toward NAA.

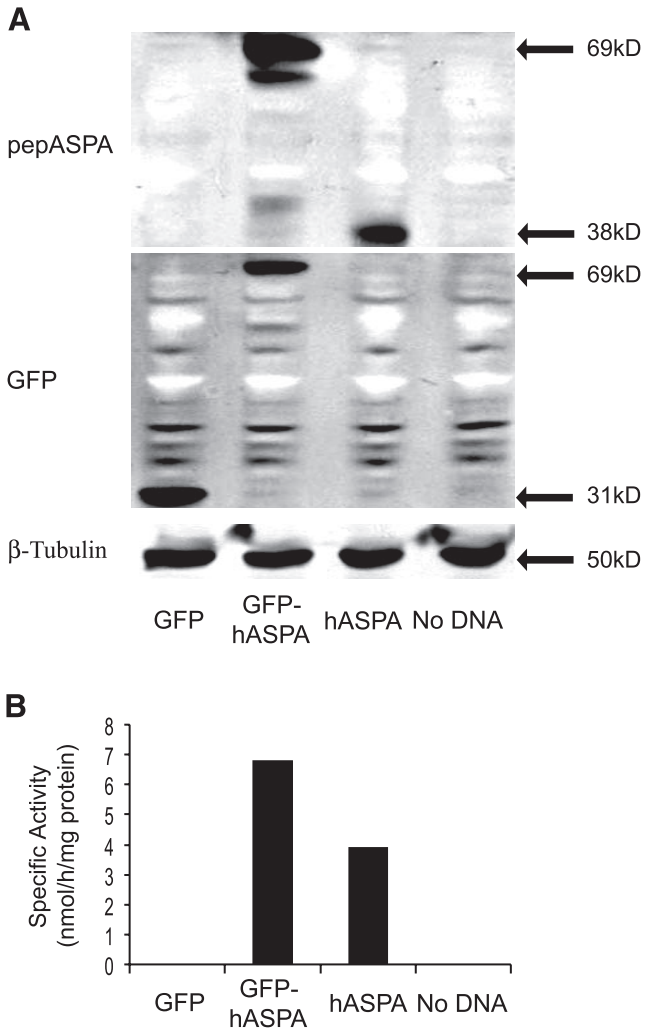

Figure 8. GFP-hASPA fusion protein is enzymatically active. Whole cell extracts were prepared from COS-7 cells transiently transfected with the indicated vectors (see Materials and Methods). *A)* Western blots with pepASPA Ab (1:5000) and a monoclonal GFP Ab (1:5000) reveal native hASPA is 38 kD, GFP alone is 31 kD, and GFP-hASPA is 69 kD. ASPA is not endogenous to COS-7 cells; 30 μg protein per lane. *B)* GFP-hASPA and native untagged hASPA have comparable activities using the radiometric ASPA enzyme assay.

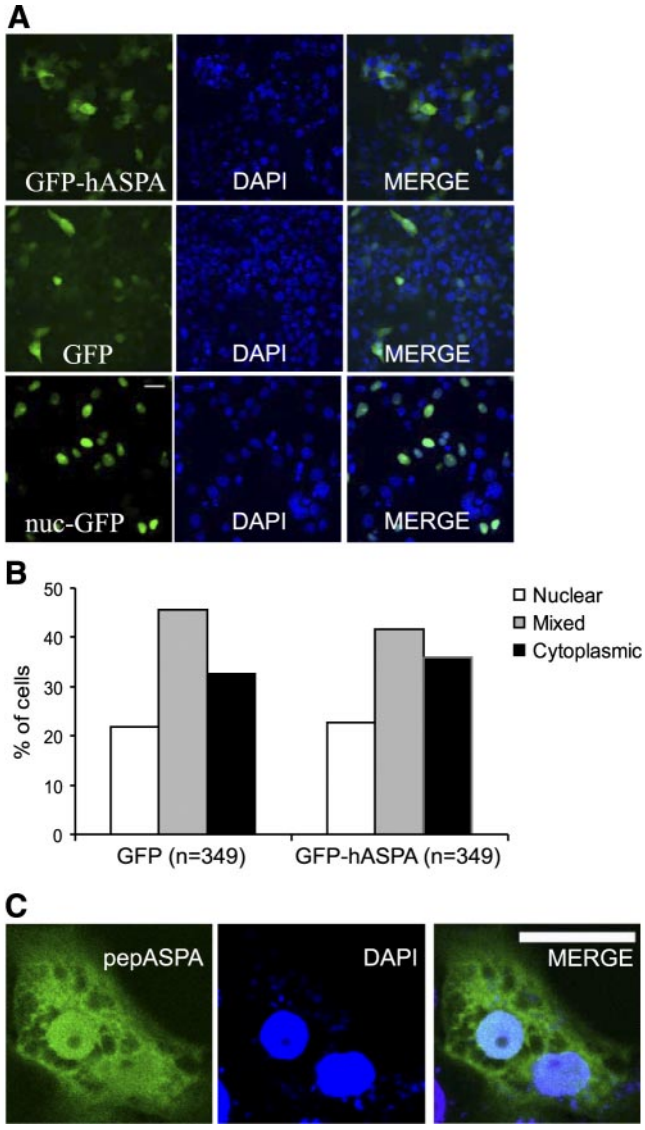

Figure 9. Transfected GFP-hASPA and native hASPA are nuclear-cytoplasmic. COS-7 cells were transiently transfected with the indicated vectors. *A)* Confocal microscopy of representative fields. Cells were grown and fixed on coverslips. GFP-hASPA depicts mostly mixed nuclear-cytoplasmic staining. GFP depicts mixed staining and nuc-GFP (GFP targeted to the nucleus by the SV40 Large T antigen NLS) depicts predominantly nuclear localization. Scale bar = 20 μm. *B)* Quantification of GFP-hASPA subcellular distribution. Several fields of cells grown in 24-well plates and imaged directly by using an inverted fluorescent microscope were scored for mainly nuclear, mixed nuclear-cytoplasmic, and mainly cytoplasmic localization based on merged images with DAPI. GFP-hASPA is predominantly nuclear-cytoplasmic, similar to the GFP control. *C)* Indirect immunofluorescence of native untagged hASPA. Fixed cells were stained using pepASPA Ab (1:1000), visualized by FITC-conjugated secondary Ab, and imaged by confocal microscopy (see Materials and Methods). Representative cells display ASPA distributed throughout cytoplasm while colocalizing with DAPI in two representative fields at high magnification. Scale bar = 10 μm.

Three additional arguments support this unexpected localization for ASPA. First, both ASPA antibodies, one directed to a conserved peptide region (pepASPA) and the other directed against the whole protein (αASPA), gave the same nuclear pattern of staining in cultured oligodendrocytes from both rat and mouse. Second, specificity of the αASPA signal seen in tissue sections was confirmed using corresponding brain and kidney sections from *Tremor* rats (28) wherein ASPA staining was completely absent. Third, expression of both GFP-tagged and native untagged human ASPA in COS-7 cells showed a mixed nuclear-cytoplasmic distribution.

Analysis of the GFP-hASPA fusion protein, which was larger than the 40–60 kD cutoff for passive diffusion through the NPC (36), demonstrated active import of ASPA into the nucleus. We now consider ASPA a member of a burgeoning family of previously assumed cytoplasmic proteins also capable of nuclear localization, including receptor interacting protein 3 (41), choline acetyltransferase (42), and nardilysin (39).

Moreover, ASPA appears to be similar to proteins such as proteinase inhibitor 9 (43), histones (36, 44), high mobility group proteins (44), and the 18 kD isoform of fibroblast growth factor 2 (45), which are small enough to passively diffuse through the NPC but have been shown to be actively imported.

The functional significance of nuclear ASPA in brain oligodendrocytes and kidney proximal tubule cells remains unknown, yet highly intriguing. One recently confirmed function of ASPA in brain is to supply acetyl groups from NAA for myelin lipid synthesis (14). This role is consistent with the dysmyelination observed in CD patients with mutations that ablate ASPA's catalytic activity (46). We confirm in this report that ASPA is expressed predominantly in oligodendrocytes in the CNS (8, 15, 16). We observed nuclear ASPA staining only in a subpopulation of predominantly immature oligodendrocytes in cell culture, raising the possibility that ASPA's subcellular localization is regulated during oligodendrocyte development and/or myelination. In the future, a closer examination of ASPA staining during rodent development may provide insight into whether nuclear ASPA follows the same expression pattern as cytoplasmic ASPA, or if pools of ASPA are sequestered in the nucleus in order to regulate free acetyl groups for myelin lipid synthesis.

The functions served by ASPA in the CNS have been fairly well studied; however, the physiological role of ASPA within kidney has yet to be closely examined. Although kidney ASPA was the original source for ASPA purification from hog (47) and is more abundant than brain ASPA and much more active against NAA (6, 19), it has been assigned a simple scavenging function (19). While molecular diagnosis is currently required as confirmation (48), elevated urine NAA remains as the fundamental diagnostic marker of children with CD (46). This raises the possibility that kidney ASPA serves a crucial role in deacetylating NAA retained from the circulation (49). In CD patients, dysfunctional proximal tubule ASPA could result in impaired ability to deacetylate retained NAA, resulting in its accumulation in urine where it is easily detectable. The cause of this accumulation has yet to be investigated and could be due to dysfunctional kidney, increased pathological NAA clearance from the circulation, or both. Curiously, kidney pathology is rarely reported in children with CD (28, 50). It is possible that one function of ASPA in kidney is to retain acetate from small acetylated compounds in the circulation via deacetylation. Loss of ASPA function in the kidney could then exacerbate the reduced acetate availability involved in the pathogenesis of CD (14). There are two other partially characterized aminoacylases in kidney with residual specificity toward NAA (33, 34), which may assist with ASPA's physiological role in kidney. In this report we localized ASPA to proximal tubules of kidney cortex, noting that ASPA was absent from the entire kidney medulla, as well as the cortical glomeruli. Acylases are generally abundant in kidney, and both aminoacylase I and III have been localized to kidney proximal tubules (33, 34), similar to the distribution of ASPA (aminoacylase II) observed in the current study. Acylases purportedly function in the detoxification of xenobiotic compounds. Another possible implication of ASPA localization to these kidney regions is retention of amino acids, a known function of the kidney proximal tubules.

At least two possibilities pertain to the reduced catalytic activity of nuclear ASPA toward NAA. First, a small pool of ASPA is targeted to the nucleus by a hereto unknown regulatory signal and retains catalytic activity against NAA. The mostly cytoplasmic 69 kD form of choline acetyltransferase, which catalyzes synthesis of the neurotransmitter acetylcholine (Ach), was found to retain minimal activity in fractionated nuclei of transiently transfected HEK293 cells (51). Second, when ASPA is targeted to nuclei, either the nuclear environment or some modification to the enzyme causes it to lose most of its specificity toward NAA. Enzymes such as CMP-Neu5Ac-synthetase, which catalyzes the activation of 5-N-acetylneuraminic acid to cytidine-monophosphate N-acetylneuraminic acid (52), and the 82 kD isoform of choline acetyltransferase (42) are believed to have alternate nuclear substrate specificities. This supports the hypothesis that ASPA has an alternate specificity when nuclear. In addition to possibly being active against other N-acetylated amino acids, nuclear ASPA may also be active against N-acetylated proteins such as actin, which in its active form has an acetylated aspartate as its N-terminal residue (53, 54). It is known that actin is present in the nucleus (55) and that its binding activity to myosin is regulated by an N-terminal acetylation/deacetylation mechanism (56). The fact that ASPA activity against NAA was relatively low in nuclear extracts, whereas ASPA immunoreactivity was generally strong in kidney and oligodendrocytes nuclei, further suggests that nuclear ASPA may have different substrate specificities than the cytoplasmic form.

It is difficult to reconcile the low nuclear ASPA expression as shown by Western blot with the strong nuclear staining for ASPA observed by immunohistochemistry in oligodendrocytes and proximal kidney tubule cells. One possibility is that the isolation and preparation of tissue nuclei for Western blotting resulted in poor ASPA yields, thus underestimating the proportion of ASPA that was localized to the nuclear compartment. Another possibility is that nuclear ASPA has a different substrate specificity and may not have high activity against NAA. It is possible that Western blotting and enzyme assays of nuclear extracts underestimated the degree of ASPA protein expression in cell nuclei.

Investigating column elution properties of cytoplasmic and nuclear ASPA elucidated another important finding of our study, which is that ASPA is active as a monomer. In previous studies, ASPA was inferred to be a dimer by mass spectroscopy of recombinant human ASPA purified from *E. coli* (20) and from Western blot analyses (8). Our current study is the first to examine native ASPA from animal tissue by size-exclusion chro-

matography, allowing us to observe that native ASPA is active as a monomer. ASPA is thus distinguished from aminoacylase III, which, through similar means, was demonstrated to be active as a tetramer (33). These data, however, do not rule out the possibility that ASPA also exists as an inactive dimer. Western blot analysis detected the majority of cytoplasmic ASPA in fractions between 29 and 45 kD, indicating that the majority of rat kidney ASPA exists as a monomer. Similarly, although we detected an ~82 to 84 kD band by Western blot analysis as previously reported (8), this band was also detected in extracts from ASPA null *Tremor* rats and in untransfected COS-7 cells, implying it was a cross-reactive protein and was not due to ASPA.

We also observed that nuclear ASPA displays less affinity toward positively charged column resins than cytoplasmic ASPA. Although this may be a trivial reflection of the different ionic environments of the extracts, it suggests that nuclear ASPA is less anionic than cytoplasmic ASPA, possibly signifying differential post-translational modifications. Mass spectroscopy analysis of recombinant human ASPA purified from *E. coli* found no posttranslational modifications (20). However, bacterially expressed proteins often do not undergo posttranslational medications that occur in eukaryotic cells. Thus, it is possible that differential phosphorylation may be involved in the nuclear localization of ASPA. We are currently investigating whether any of five putative phosphorylation target residues (19) affect ASPA activity and subcellular localization.

The mechanism responsible for the nuclear import of ASPA is currently unknown due to the lack of studies on its posttranslational regulation. Traditional protein nuclear import relies on the classical NLS (based on the SV40 large T antigen), whose critical lysine residues facilitate protein binding to importin α/importin β for movement through the NPC (57, 58). However, there are a wealth of less-characterized sequences for nuclear targeting, including a 38 amino acid fragment from hnRNP A1 and A2 (M9 sequence), the KNS sequence from hnRNP K protein, the HNS sequence from the HuR protein, ankyrin repeats from IkBalpha, an acidic amino acid region in FAS associated factor 1, a PPXXR sequence of Sam68, a S/TPXKRL/I sequence of Cdc6, and GR repeats in large FGF-2 isoforms (44). Most notably, an experimental approach to discovering novel NLS's found less than 50% of the classical variety as well as several sequences exhibiting clusters of just 2–3 lysine and/or arginine nonbipartite basic NLS repeats and RTRG repeats (44). Indeed, not all nuclear proteins need an NLS as entry may be afforded by interaction with another protein that does have an NLS (36). Conversely, an NLS does not guarantee nuclear localization as 4.2% of non-nuclear proteins contain a putative NLS (59). Epitope masking, glycosylation, and phosphorylation are other ways for proteins lacking an NLS to enter the nucleus (59). Visual inspection after failing to find a putative or functional NLS has identified a nonclassical C-terminal bipartite NLS in 18 kD fibroblast growth factor-2, characterized by two clusters of two or three basic amino acids separated by 8–17 amino acids (40). Similarly, we searched ASPA's primary amino acid sequence for clusters of conserved basic amino acids and identified a conserved KKEAFAKTTK C-terminal sequence. This putative NLS resembles a functional nonclassical NLS, PAAKRVKLD (60) and is a condensed version of a nonclassical bipartite NLS found in SIM1 and SIM2 proteins (61). We are currently assessing the importance of this region of ASPA in influencing partial nuclear localization.

In summary, we have shown that ASPA is localized to both cytoplasm and the nucleus in specific cell types in rodent brain and kidney and that this nuclear enzyme is weakly catalytically active against the only known substrate for the cytoplasmic form of the enzyme. Concurrently, we have shown that ASPA is active as a monomer and that nuclear import is not due to simple diffusion. The biological role of nuclear ASPA remains to be established. It is possible that CD mutations in ASPA affect its subcellular localization in addition to its catalytic activity and that variations in the two might play a critical role in determining different CD phenotypes. Thus, regulation of ASPA's nuclear-cytoplasmic shuttling could be highly significant in understanding both the molecular basis for, and the potential treatment of CD. FJ

The research was supported by the NIH grant NS 39387 to M.A.A.N. and the National Multiple Sclerosis Society grant RG3204 to J.Y.G. and J.R.B. We are grateful to Dr. Paula Leone and Dr. Scott McPhee at the Department of Surgery at UMDNJ and to Dr. Tadao Serikawa at The Institute of Laboratory Animals at the Graduate School of Medicine, Kyoto University, Japan for providing *Tremor* and WT rat organs. We thank Dr. Regina Armstrong for critical analyses of the nuclear localization data as well as for providing primary cultures of oligodendrocytes along with Dr. Josh Murtie and Liljana Nedelkoska. Special thanks to Dr. Peethambaran Arun and Nicole Flint for assistance with cell culture and microscopy, respectively.

REFERENCES

1. Matalon, R., Michals, K., Sebesta, D., Deanching, M., Gashkoff, P., and Casanova, J. (1988) Aspartoacylase deficiency and N-acetylaspartic aciduria in patients with Canavan disease. *Am. J. Med. Genet.* **29,** 463–471
2. Leone, P., Janson, C. G., McPhee, S. J., and During, M. J. (1999) Global CNS gene transfer for a childhood neurogenetic enzyme deficiency: Canavan disease. *Curr. Opin. Mol. Ther.* **1,** 487–492
3. Kirmani, B. F., Jacobowitz, D. M., and Namboodiri, M. A. (2003) Developmental increase of aspartoacylase in oligodendrocytes parallels CNS myelination. *Brain Res. Dev. Brain Res.* **140,** 105–115
4. Bhakoo, K. K., Craig, T. J., and Styles, P. (2001) Developmental and regional distribution of aspartoacylase in rat brain tissue. *J. Neurochem.* **79,** 211–220
5. D'Adamo, A. F., Jr., Gidez, L. I., and Yatsu, F. M. (1968) Acetyl transport mechanisms. Involvement of N-acetyl aspartic acid in de novo fatty acid biosynthesis in the developing rat brain. *Exp. Brain Res.* **5,** 267–273
6. D'Adamo, A. F., Jr., Smith, J. C., and Woiler, C. (1973) The occurrence of N-acetylaspartate amidohydrolase (aminoacylase II) in the developing rat. *J. Neurochem.* **20,** 1275–1278

7. Kirmani, B. F., Jacobowitz, D. M., Kallarakal, A. T., and Namboodiri, M. A. (2002) Aspartoacylase is restricted primarily to myelin synthesizing cells in the CNS: therapeutic implications for Canavan disease. *Brain Res. Mol. Brain Res.* **107,** 176–182
8. Klugmann, M., Symes, C. W., Klaussner, B. K., Leichtlein, C. B., Serikawa, T., Young, D., and During, M. J. (2003) Identification and distribution of aspartoacylase in the postnatal rat brain. *Neuroreport* **14,** 1837–1840
9. Benuck, M., and D'Adamo, A. F., Jr. (1968) Acetyl transport mechanisms. Metabolism of N-acetyl-L-aspartic acid in the nonnervous tissues of the rat. *Biochim. Biophys. Acta* **152,** 611–618
10. Burri, R., Steffen, C., and Herschkowitz, N. (1991) N-acetyl-L-aspartate is a major source of acetyl groups for lipid synthesis during rat brain development. *Dev. Neurosci.* **13,** 403–411
11. Chakraborty, G., Mekala, P., Yahya, D., Wu, G., and Ledeen, R. W. (2001) Intraneuronal N-acetylaspartate supplies acetyl groups for myelin lipid synthesis: evidence for myelin-associated aspartoacylase. *J. Neurochem.* **78,** 736–745
12. D'Adamo, A. F., Jr., and Yatsu, F. M. (1966) Acetate metabolism in the nervous system. N-acetyl-L-aspartic acid and the biosynthesis of brain lipids. *J. Neurochem.* **13,** 961–965
13. Mehta, V., and Namboodiri, M. A. (1995) N-acetylaspartate as an acetyl source in the nervous system. *Brain Res. Mol. Brain Res.* **31,** 151–157
14. Madhavarao, C. N., Arun, P., Moffett, J. R., Szucs, S., Surendran, S., Matalon, R., Garbern, J., Hristova, D., Johnson, A., Jiang, W., and Namboodiri, M. A. (2005) Defective N-acetylaspartate catabolism reduces brain acetate levels and myelin lipid synthesis in Canavan's disease. *Proc. Natl. Acad. Sci. U. S. A.* **102,** 5221–5226
15. Baslow, M. H., Suckow, R. F., Sapirstein, V., and Hungund, B. L. (1999) Expression of aspartoacylase activity in cultured rat macroglial cells is limited to oligodendrocytes. *J. Mol. Neurosci.* **13,** 47–53
16. Madhavarao, C. N., Moffett, J. R., Moore, R. A., Viola, R. E., Namboodiri, M. A., and Jacobowitz, D. M. (2004) Immunohistochemical localization of aspartoacylase in the rat central nervous system. *J. Comp. Neurol.* **472,** 318–329
17. D'Adamo, A. F., Jr., Wertman, E., Foster, F., and Schneider, H. (1978) A radiochemical assay for N-acetyl-L-aspartate amidohydrolase (EC 3.5.1.15) and its occurrence in the tissues of the chicken. *Life Sci.* **23,** 791–795
18. Kaul, R., Casanova, J., Johnson, A. B., Tang, P., and Matalon, R. (1991) Purification, characterization, and localization of aspartoacylase from bovine brain. *J. Neurochem.* **56,** 129–135
19. Kaul, R., Gao, G. P., Balamurugan, K., and Matalon, R. (1993) Cloning of the human aspartoacylase cDNA and a common missense mutation in Canavan disease. *Nat. Genet.* **5,** 118–123
20. Moore, R. A., Le Coq, J., Faehnle, C. R., and Viola, R. E. (2003) Purification and preliminary characterization of brain aspartoacylase. *Arch. Biochem. Biophys.* **413,** 1–8
21. Armstrong, R. C. (1998) Isolation and characterization of immature oligodendrocyte lineage cells. *Methods* **16,** 282–292
22. Linnington, C., Webb, M., and Woodhams, P. L. (1984) A novel myelin-associated glycoprotein defined by a mouse monoclonal antibody. *J. Neuroimmunol.* **6,** 387–396
23. Benjamins, J. A., Nedelkoska, L., and George, E. B. (2003) Protection of mature oligodendrocytes by inhibitors of caspases and calpains. *Neurochem. Res.* **28,** 143–152
24. McCarthy, K. D., and de Vellis, J. (1980) Preparation of separate astroglial and oligodendroglial cell cultures from rat cerebral tissue. *J. Cell Biol.* **85,** 890–902
25. Fleming, M. C., and Lowry, O. H. (1966) The measurement of free and N-acetylated aspartic acids in the nervous system. *J. Neurochem.* **13,** 779–783
26. Madhavarao, C. N., Hammer, J. A., Quarles, R. H., and Namboodiri, M. A. (2002) A radiometric assay for aspartoacylase activity in cultured oligodendrocytes. *Anal. Biochem.* **308,** 314–319
27. Namboodiri, M. A., Corigliano-Murphy, A., Jiang, G., Rollag, M., and Provencio, I. (2000) Murine aspartoacylase: cloning, expression and comparison with the human enzyme. *Brain Res. Mol. Brain Res.* **77,** 285–289
28. Kitada, K., Akimitsu, T., Shigematsu, Y., Kondo, A., Maihara, T., Yokoi, N., Kuramoto, T., Sasa, M., and Serikawa, T. (2000) Accumulation of N-acetyl-L-aspartate in the brain of the tremor rat, a mutant exhibiting absence-like seizure and spongiform degeneration in the central nervous system. *J. Neurochem.* **74,** 2512–2519
29. Yamada, J., Serikawa, T., Ishiko, J., Inui, T., Takada, H., Kawai, Y., and Okaniwa, A. (1985) Rats with congenital tremor and curled whiskers and hair. *Jikken Dobutsu.* **34,** 183–188
30. Matalon, R., Rady, P. L., Platt, K. A., Skinner, H. B., Quast, M. J., Campbell, G. A., Matalon, K., Ceci, J. D., Tyring, S. K., Nehls, M., and Surendran, S., *et al.* (2000) Knock-out mouse for Canavan disease: a model for gene transfer to the central nervous system. *J. Gene Med.* **2,** 165–175
31. Moffett, J. R., Namboodiri, M. A., Cangro, C. B., and Neale, J. H. (1991) Immunohistochemical localization of N-acetylaspartate in rat brain. *Neuroreport.* **2,** 131–134
32. Birnbaum, S. M. (1955) Amino acid acylases I and II from hog kidney. *Methods Enzymol.* **2,** 115–119
33. Pushkin, A., Carpenito, G., Abuladze, N., Newman, D., Tsuprun, V., Ryazantsev, S., Motemoturu, S., Sassani, P., Solovieva, N., Dukkipati, R., and Kurtz, I. (2004) Structural characterization, tissue distribution, and functional expression of murine aminoacylase III. *Am. J. Physiol. Cell Physiol.* **286,** C848–856
34. Uttamsingh, V., Baggs, R. B., Krenitsky, D. M., and Anders, M. W. (2000) Immunohistochemical localization of the acylases that catalyze the deacetylation of N-acetyl-L-cysteine and haloalkene-derived mercapturates. *Drug Metab. Dispos.* **28,** 625–632
35. Cook, R. M., Burke, B. J., Buchhagen, D. L., Minna, J. D., and Miller, Y. E. (1993) Human aminoacylase-1. Cloning, sequence, and expression analysis of a chromosome 3p21 gene inactivated in small cell lung cancer. *J. Biol. Chem.* **268,** 17010–17017
36. Nigg, E. A. (1997) Nucleocytoplasmic transport: signals, mechanisms and regulation. *Nature* **386,** 779–787
37. Elpeleg, O. N., and Shaag, A. (1999) The spectrum of mutations of the aspartoacylase gene in Canavan disease in non-Jewish patients. *J. Inherit. Metab. Dis.* **22,** 531–534
38. Kaul, R., Gao, G. P., Aloya, M., Balamurugan, K., Petrosky, A., Michals, K., and Matalon, R. (1994) Canavan disease: mutations among Jewish and non-Jewish patients. *Am. J. Hum. Genet.* **55,** 34–41
39. Ma, Z., Chow, K. M., Yao, J., and Hersh, L. B. (2004) Nuclear shuttling of the peptidase nardilysin. *Arch. Biochem. Biophys.* **422,** 153–160
40. Sheng, Z., Lewis, J. A., and Chirico, W. J. (2004) Nuclear and nucleolar localization of 18-kDa fibroblast growth factor-2 is controlled by C-terminal signals. *J. Biol. Chem.* **279,** 40153–40160
41. Yang, Y., Ma, J., Chen, Y., and Wu, M. (2004) Nucleocytoplasmic shuttling of receptor-interacting protein 3 (RIP3): identification of novel nuclear export and import signals in RIP3. *J. Biol. Chem.* **279,** 38820–38829
42. Resendes, M. C., Dobransky, T., Ferguson, S. S., and Rylett, R. J. (1999) Nuclear localization of the 82-kDa form of human choline acetyltransferase. *J. Biol. Chem.* **274,** 19417–19421
43. Bird, C. H., Blink, E. J., Hirst, C. E., Buzza, M. S., Steele, P. M., Sun, J., Jans, D. A., and Bird, P. I. (2001) Nucleocytoplasmic distribution of the ovalbumin serpin PI-9 requires a nonconventional nuclear import pathway and the export factor Crm1. *Mol. Cell. Biol.* **21,** 5396–5407
44. Christophe, D., Christophe-Hobertus, C., and Pichon, B. (2000) Nuclear targeting of proteins: how many different signals? *Cell Signal* **12,** 337–341
45. Foletti, A., Vuadens, F., and Beermann, F. (2003) Nuclear localization of mouse fibroblast growth factor 2 requires N-terminal and C-terminal sequences. *Cell Mol. Life Sci.* **60,** 2254–2265
46. Matalon, R., and Michals-Matalon, K. (1999) Biochemistry and molecular biology of Canavan disease. *Neurochem. Res.* **24,** 507–513
47. Birnbaum, S. M., Levintow, L., Kingsley, R. B., and Greenstein, J. P. (1952) Specificity of amino acid acylases. *J. Biol. Chem.* **194,** 455–470
48. Besley, G. T., Elpeleg, O. N., Shaag, A., Manning, N. J., Jakobs, C., and Walter, J. H. (1999) Prenatal diagnosis of Canavan disease–problems and dilemmas. *J. Inherit. Metab. Dis.* **22,** 263–266
49. Clark, J. B. (1998) N-acetyl aspartate: a marker for neuronal loss or mitochondrial dysfunction. *Dev. Neurosci.* **20,** 271–276
50. Leone, P., Janson, C. G., Bilaniuk, L., Wang, Z., Sorgi, F., Huang, L., Matalon, R., Kaul, R., Zeng, Z., and Freese, A., *et al.* (2000) Aspartoacylase gene transfer to the mammalian central

nervous system with therapeutic implications for Canavan disease. *Ann. Neurol.* **48,** 27–38
51. Gill, S. K., Bhattacharya, M., Ferguson, S. S., and Rylett, R. J. (2003) Identification of a novel nuclear localization signal common to 69- and 82-kDa human choline acetyltransferase. *J. Biol. Chem.* **278,** 20217–20224
52. Munster, A. K., Weinhold, B., Gotza, B., Muhlenhoff, M., Frosch, M., and Gerardy-Schahn, R. (2002) Nuclear localization signal of murine CMP-Neu5Ac synthetase includes residues required for both nuclear targeting and enzymatic activity. *J. Biol. Chem.* **277,** 19688–19696
53. Rubenstein, P. A., and Martin, D. J. (1983) NH2-terminal processing of actin in mouse L-cells in vivo. *J. Biol. Chem.* **258,** 3961–3966
54. Rubenstein, P. A., and Martin, D. J. (1983) NH2-terminal processing of Drosophila melanogaster actin. Sequential removal of two amino acids. *J. Biol. Chem.* **258,** 11354–11360
55. Pederson, T., and Aebi, U. (2002) Actin in the nucleus: what form and what for? *J. Struct. Biol.* **140,** 3–9
56. Abe, A., Saeki, K., Yasunaga, T., and Wakabayashi, T. (2000) Acetylation at the N-terminus of actin strengthens weak interaction between actin and myosin. *Biochem. Biophys. Res. Commun.* **268,** 14–19
57. Kuersten, S., Ohno, M., and Mattaj, I. W. (2001) Nucleocytoplasmic transport: Ran, beta and beyond. *Trends Cell Biol.* **11,** 497–503
58. Yoneda, Y. (2000) Nucleocytoplasmic protein traffic and its significance to cell function. *Genes Cells* **5,** 777–787
59. Dingwall, C., and Laskey, R. A. (1991) Nuclear targeting sequences–a consensus? *Trends Biochem. Sci.* **16,** 478–481
60. Makkerh, J. P., Dingwall, C., and Laskey, R. A. (1996) Comparative mutagenesis of nuclear localization signals reveals the importance of neutral and acidic amino acids. *Curr. Biol.* **6,** 1025–1027
61. Yamaki, A., Kudoh, J., Shimizu, N., and Shimizu, Y. (2004) A novel nuclear localization signal in the human single-minded proteins SIM1 and SIM2. *Biochem. Biophys. Res. Commun.* **313,** 482–488

Received for publication January 4, 2006.
Accepted for publication May 25, 2006.